water

MDPI

Article

Evaluation of Long-Term Impacts of CO_2 Leakage on Groundwater Quality Using Hydrochemical Data from a Natural Analogue Site in South Korea

Hyun-Kwon Do [1], Seong-Taek Yun [1,*], Soonyoung Yu [1], Yon-Gyung Ryuh [2] and Hyeon-Su Choi [3]

1 Department of Earth and Environmental Sciences and Korea CO_2 Storage Environmental Management (K-COSEM) Research Center, Korea University, Seoul 02841, Korea; iq1pc@korea.ac.kr (H.-K.D.); iamysy@korea.ac.kr (S.Y.)
2 Department of Earth and Environmental Sciences, University of Waterloo, Waterloo, ON N2L 3G1, Canada; yryuh@uwaterloo.ca
3 ENGI Inc., Seongnam, Gyeonggi 13511, Korea; isotope1@daum.net
* Correspondence: styun@korea.ac.kr; Tel.: +82-2-3290-3176

Received: 6 April 2020; Accepted: 19 May 2020; Published: 20 May 2020

Abstract: Three hydrochemical types of CO_2-rich water (i.e., Na-HCO_3, Ca-Na-HCO_3 and Ca-HCO_3) occur together in the silicate bedrock (granite and gneiss) of Gangwon Province in South Korea. As a natural analogue of geological carbon storage (GCS), this can provide implications for the environmental impacts of the leakage of CO_2 from deep GCS sites. By using hydrochemical and isotopic datasets that were collected for previous and current studies, this study aimed to carefully scrutinize the hydrochemical differences in the three water types with an emphasis on providing a better understanding of the impacts of long-term CO_2 leakage on groundwater quality (especially the enrichments of minor and trace metals). As a result, the Na-HCO_3 type CO_2-rich water contained higher Li, Rb and Cs than the Ca-HCO_3 type, whereas Fe, Mn and Sr were higher in the Ca-HCO_3 type than in the Na-HCO_3 type despite the similar geological setting, which indicate that the hydrochemical differences were caused during different geochemical evolutionary processes. The $\delta^{18}O$ and δD values and tritium concentrations indicated that the Na-HCO_3 type was circulated through a deep and long pathway for a relatively long residence time in the subsurface, while the Ca-HCO_3 type was strongly influenced by mixing with recently recharged water. These results were supported by the results of principal component analysis (PCA), whose second component showed that the Na-HCO_3 type had a significant relation with alkali metals such as Li, Rb and Cs as well as Na and K and also had a strong relationship with Al, F and U, indicating an extensive water-rock interaction, while the Ca-HCO_3 type was highly correlated with Ca, Mg, Sr, Fe and Mn, indicating mixing and reverse cation exchange during its ascent with hydrogeochemical evolution. In particular, the concentrations of Fe, Mn, U and Al in the CO_2-rich water, the result of long-term water-rock interaction and cation exchange that was enhanced by CO_2 leakage into silicate bedrock, exceeded drinking water standards. The study results show that the leakage of CO_2 gas and CO_2-rich fluid into aquifers and the subsequent hydrogeochemical processes can degrade groundwater quality by mobilizing trace elements in rocks and consequently may pose a health risk.

Keywords: CO_2 leakage; long-term impact; groundwater quality; trace metal; natural analogue

1. Introduction

Carbon dioxide stored in geological carbon storage (GCS) sites can migrate upwards from a storage reservoir through various paths such as faults, fractures, small cracks in caprocks, and

borehole annulus [1–5]. Even though GCS is a promising technology for substantially reducing CO_2 emissions [6,7], such migration of CO_2 gas and CO_2-rich fluid into freshwater aquifers may lead to the degradation of potable groundwater by total dissolved solids and trace metals, and moreover the leakage itself means the failure of net CO_2 reduction [8–11]. Therefore, accurate monitoring of CO_2 leakage into potable aquifers is crucial for the successful, safe and long-term storage of CO_2. Among various groundwater monitoring methods, hydrochemical and isotopic analyses have been widely used to detect CO_2 leakage and evaluate its potential impact on groundwater quality [9,12–14].

The extent and rate of hydrogeochemical reactions caused by the inflow of CO_2 may differ depending on the geological and geochemical conditions of aquifers [12,15–17]. Therefore, to find a geochemical index for CO_2 leakage detection and to evaluate the impact of CO_2 leakage on groundwater quality, the hydrochemical responses to the inflow of CO_2 into aquifers have been studied in various ways such as in laboratory experiments [1,10,18,19], controlled CO_2 injection field tests [9–12,20,21], and natural analogues [8,15,22–24]. A natural analogue study with CO_2-rich water is the best way to observe the hydrochemical changes caused by a long period of CO_2 supply [8,12]. The hydrochemical and isotopic data of CO_2-rich water improve our understanding of the potential risks associated with the long-term leakage and migration of CO_2 into potable aquifers.

In this study, careful reevaluations of hydrochemical and isotopic data of CO_2-rich water were conducted in a natural analogue site in South Korea (Figure 1) to evaluate the long-term impact of CO_2 leakage on groundwater quality in silicate bedrock areas. In particular, the levels of trace elements were investigated with respect to hydrogeochemical processes depending on water types to understand the relationship between geochemical processes and water quality in GCS sites. It should be noted that CO_2-rich water in the study area has been partly or wholly studied by the current authors [25–27] and others [28,29]. However, the previous studies focused on the identification of geochemical processes causing hydrochemical differences in CO_2-rich water, and did not evaluate the impact of leaked CO_2 on minor and trace elements in CO_2-rich water, although the increases in trace element levels can deteriorate the groundwater quality in potable aquifers [8,24,30].

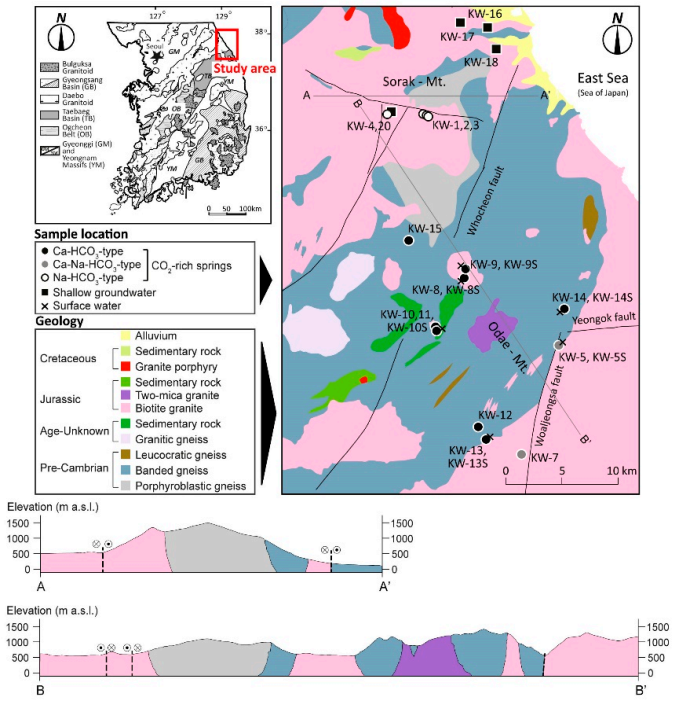

Figure 1. Geological map with cross sections (A-A′ and B-B′) of the northeastern part of Gangwon Province, South Korea, with the locations of CO_2-rich water (circles), shallow groundwater (squares) and surface water (crosses) (modified after Choi et al. [25]). The water types were classified based on the Piper diagram (see below).

2. Study Area

The study area, Gangwon Province, is located in the northeastern part of South Korea (Figure 1). The geology consists mainly of Precambrian gneisses, Jurassic sedimentary rocks and Mesozoic granitoids. The Mesozoic granitoids contain biotite granite, two-mica granite and porphyry, while the Precambrian gneisses occupying the central part of the study area can be grouped into porphyroblastic, banded and leucocratic gneiss [25,31]. The banded gneiss is widely exposed in the study area and shows ptygmatic folding structures and leucocratic gneiss facies [32]. The Jurassic fine-grained biotite granite is present as small intrusions, whereas the biotite granite is intruded into the banded gneiss as a large batholith (Figure 1).

The major geological structures in the study area are the Whocheon fault (in the center of Figure 1), the Woaljeongsa fault (in the southeastern part), the Yeongok fault (in the eastern part) and unnamed faults (Figure 1). The Whocheon, Woaljeongsa and unnamed faults are aligned from northeast to southwest on the Korean Peninsula, formed during the late Cretaceous, and predate the Yeongok fault that is aligned in the east-west direction [25,33]. The study area is characterized by steep mountain slopes. Mt. Sorak and Mt. Odae have an elevation exceeding 1000 m above sea level (Figure 1). The steep topography, with a relief of more than 1000 m between mountaintops and foothills, causes great hydraulic gradients and in turn possibly large circulation depths of groundwater in the study area.

As described by Choi et al. [25], CO_2-rich water typically occurs within the biotite granites of the Jurassic period and in the vicinity of the Jurassic biotite granite and the Precambrian gneiss, and the occurrence of CO_2-rich water seems to be closely related to faults (Whocheon, Woaljeongsa and unnamed faults) aligned in the northeast-southwest direction (Figure 1). In fact, the CO_2-rich water normally flows out as springs adjacent to the valleys formed by such faults [25,26].

3. Sampling and Analyses

Water samples were obtained during several sampling campaigns from August to October in 1998, July 1999, February, September and October in 2000, April in 2002, and November in 2010 for hydrochemical and isotopic analyses. A total of 44 water samples were collected from 14 CO_2-rich springs (n = 32), four shallow groundwater wells (n = 6) and streams (n = 6) in the vicinity of the CO_2-rich springs (Figure 1). In addition, 16 rock samples were taken from outcrops around the CO_2-rich springs for chemical composition analysis to see the geological effect on the hydrochemistry of CO_2-rich springs.

Temperature, pH, redox potential (Eh), electrical conductivity (EC) and dissolved oxygen (DO) of water samples were measured on-site with a portable multiparameter meter (Orion 1230) within a flow-through cell to minimize the impact of atmospheric oxygen. Alkalinity was determined on-site by titration with HCl solution (0.5N and 0.05N) as soon as the water was sampled to minimize CO_2 degassing from the CO_2-rich water. All water samples were filtered. Then the samples were acidified for major cation and minor/trace element analyses. Dissolved inorganic carbon (DIC) was precipitated using $BaCl_2$ for the carbon isotopic composition ($\delta^{13}C$) analysis of water samples.

Major cations (Na, K, Mg, Ca) and SiO_2 were determined using ICP-AES (Shimadzu, ICP-11000 III) at the Korea Basic Science Institute (KBSI). Minor to trace elements (Fe, Sr, Mn, Al, Li, B, Cr, Zn, Rb, Cs, Ba, U) were analyzed by ICP-MS (FISONS, PlasmaTrace) at KBSI. Anions (Cl, SO_4, NO_3, F) were analyzed using IC (Dionex, DX-500) at the Korea Atomic Energy Research Institute (KAERI) and the Center for Mineral Resources Research (CMR) of Korea University. Charge balance errors were within an acceptable range of ± 10% for all water samples, with most of the samples being < 5%.

The $\delta^{18}O$ and δD values of water were determined using a stable isotope ratio mass spectrometer (VG SIRA II and Micromass Optima) at KAERI by equilibrium with CO_2 gas [34] and reduction of water [35], respectively. The $\delta^{18}O$ and δD values were measured relative to the internal standards that were calibrated with V-SMOW, GISP and SLAP standards. The $\delta^{13}C$ was determined using a VG SIRA II at KAERI. The tritium concentrations of water were measured using an electrolytic enrichment process by a liquid scintillation counter (Packard Tricarb 2770SL/TR) at KAERI. The chemical compositions of rock samples were analyzed using an X-ray fluorescence spectrometer (Phillips, PW 2404) at KBSI.

In addition, the partial pressures of CO_2 (P_{CO2}) were calculated using PHREEQC software [36]. Principal component analysis (PCA) was performed using IBM SPSS Statistics for Windows, version 23 (IBM Corp., Armonk, NY, USA) to characterize major geochemical processes. PCA transforms a number of correlated variables into a smaller number of uncorrelated variables called principal components. All variables were standardized before PCA to remove the effect of scale differences in variables [37].

The results of field measurements and laboratory analyses of water samples are shown in Tables 1–3, while the results of the chemical analysis of representative rock samples are shown in Table 4. It should be noted again that some datasets for a few water and rock samples were utilized by the current authors for previous studies with different research purposes. The sources of previously used data are clearly given in each table as captions.

Table 1. Physicochemical data of water samples in the Gangwon Province of South Korea. CO_2-rich water is grouped based on the Piper diagram (see Figure 3).

Sample No. [1]	Sampling Date	Temp. (°C)	pH	Eh (mV)	EC (μS/cm)	DO (mg/L)	TDS (mg/L)	Log P_{CO2} (atm) [2]	Concentrations (mg/L)									
									Na	K	Mg	Ca	SiO_2	Cl^-	SO_4^{2-}	NO_3^-	F^-	Alk. [3]
CO_2-rich water (Na-HCO_3 type)																		
KW-1(a)	Sep-01-98	19.4	6.04	318	1345	2.6	1629	−0.02	345.0	23.0	1.6	31.5	79.6	7.0	12.9	0.1	7.5	1117
KW-1′(a, c)	Jul-07-99	18.5	6.24	326	1348	3.1	1773	−0.21	419.0	25.0	2.1	44.6	87.7	8.3	13.8	n.d.	7.7	1159
KW-1″(b)	Apr-08-02	9.6	6.38	264	1469	4.2	1641	−0.36	377.3	18.7	1.4	36.6	68.2	6.8	11.0	0.4	5.0	1113
KW-2(a)	Sep-01-98	18.7	5.85	330	1268	3.8	2014	0.23	496.0	27.3	2.2	53.1	89.0	9.5	21.8	0.1	7.1	1302
KW-2′(a, c)	Jul-07-99	18.2	6.21	337	2220	3.3	2625	0.02	544.0	32.1	2.6	57.1	93.1	2.5	22.4	n.d.	7.1	1861
KW-2‴(b)	Apr-08-02	9.9	6.36	258	1941	2.3	2215	−0.22	533.5	24.0	1.7	44.3	74.2	10.4	20.1	n.d.	4.2	1495
KW-2⁗(a)	Nov-19-10	6.1	6.31	284	2052	1.6	2118	−0.19	472.7	35.4	2.0	58.2	90.4	14.0	20.1	n.d.	n.d.	1425
KW-3	Sep-01-98	15.8	5.87	317	864	3.1	1020	−0.08	267.0	7.2	0.5	10.7	71.9	5.0	5.0	0.1	9.3	638
KW-3′	Jul-07-99	15.4	6.13	341	1058	2.8	1089	−0.30	271.0	6.1	0.5	11.0	74.0	5.6	5.1	0.1	9.5	702
KW-3‴(b, c)	Apr-08-02	11.2	6.55	235	1055	2.8	1569	−0.55	408.1	5.7	0.3	12.9	73.7	4.4	3.7	n.d.	7.4	1052
KW-4	Sep-01-98	13.4	5.85	335	1956	1.2	1846	0.21	455.0	13.0	5.2	54.0	61.0	8.3	8.0	0.1	4.9	1233
KW-4′	Jul-07-99	19.8	6.43	343	1871	1.5	1921	−0.35	457.0	10.5	5.1	53.2	60.1	8.6	7.3	n.d.	4.8	1312
KW-4‴(b, c)	Apr-08-02	9.8	6.65	237	1713	0.5	1947	−0.56	488.4	7.6	4.0	46.3	48.1	8.1	6.1	n.d.	3.1	1334
KW-4⁗	Nov-19-10	9.7	6.62	280	1837	1.2	1903	−0.54	433.7	13.0	4.6	57.8	59.5	21.7	8.8	n.d.	n.d.	1304
CO_2-rich water (Ca-Na-HCO_3 type)																		
KW-5	Jul-01-98	14.5	5.52	254	725	2.4	714	0.15	71.4	4.5	7.3	76.1	32.5	6.7	16.1	0.3	2.4	488
KW-5′	Jul-07-99	16.2	5.70	358	778	2.1	775	0.00	91.8	4.0	8.6	88.4	37.9	2.1	12.7	n.d.	2.6	519
KW-5‴(b)	Apr-08-02	17.2	5.69	282	695	1.9	696	−0.03	91.1	2.1	6.4	71.2	24.3	6.7	12.0	n.d.	1.9	473
KW-5⁗	Nov-18-10	10.4	5.91	388	990	1.3	982	−0.12	106.6	4.7	10.3	120.9	40.5	33.3	13.0	n.d.	n.d.	653
KW-7(b, c)	Apr-08-02	13.5	6.45	237	894	2.1	967	−0.66	89.7	2.4	11.9	134.2	37.5	11.2	7.9	5.4	2.7	656
CO_2-rich water (Ca-HCO_3 type)																		
KW-8(a, c)	Oct-30-98	14.4	6.04	324	1528	3.5	1464	−0.10	32.3	4.2	25.7	293.8	76.1	2.9	21.1	0.1	0.9	988
KW-8′(a)	Nov-19-10	8.4	6.12	305	1451	1.6	1510	−0.16	33.1	2.8	25.8	307.2	76.7	3.9	23.7	0.2	0.5	1036
KW-9(a, b, c)	Oct-30-98	13.3	5.51	375	454	3.8	419	−0.12	6.6	0.5	9.7	72.5	54.0	3.3	13.6	0.1	1.7	249
KW-10(a, b, c)	Oct-30-98	10.7	5.88	406	677	5.1	642	−0.29	15.0	2.7	11.9	109.7	60.8	2.6	10.5	0.3	1.5	411
KW-10″(a)	Nov-19-10	6.4	5.93	326	909	1.7	900	−0.18	20.4	2.5	17.0	163.6	75.1	4.0	16.5	n.d.	1.8	599
KW-11(b)	Apr-08-02	7.3	6.34	170	1763	1.3	1993	−0.24	49.1	2.4	45.9	348.7	73.4	5.9	12.3	n.d.	1.9	1434
KW-12	Jul-01-99	11.4	5.87	329	1034	1.6	1054	−0.02	37.0	2.3	35.4	162.0	36.0	2.3	4.3	0.1	0.6	763
KW-12′(b, c)	Apr-08-02	7.4	6.26	272	977	2.6	975	−0.45	32.6	2.5	16.2	178.3	24.9	2.7	3.9	0.3	0.3	702
KW-13	Aug-01-98	16.2	5.81	343	873	0.8	856	−0.06	14.8	1.6	36.1	140.0	35.1	2.1	9.2	0.1	0.2	598
KW-13′	Jul-07-99	10.4	5.75	393	915	0.6	964	0.06	15.5	4.6	37.2	140.0	39.2	2.3	7.8	n.d.	0.3	702
KW-14(c)	Jul-07-99	14.1	5.78	317	921	2.1	834	−0.02	15.2	2.9	46.1	93.0	30.2	2.1	7.6	n.d.	0.4	610
KW-14′(b)	Apr-08-02	8.6	5.98	269	794	2.2	841	−0.24	13.7	3.4	67.5	82.1	49.5	3.2	6.7	n.d.	0.3	589
KW-15(c)	Oct-02-99	12.4	5.46	375	1098	3.6	1141	0.41	35.9	3.3	20.9	198.1	48.4	2.9	8.2	n.d.	0.8	808

Table 1. *Cont.*

Sample No. [1]	Sampling Date	Temp. (°C)	pH	Eh (mV)	EC (μS/cm)	DO (mg/L)	TDS (mg/L)	Log P_{CO2} (atm) [2]	Concentrations (mg/L)									
									Na	K	Mg	Ca	SiO_2	Cl^-	SO_4^{2-}	NO_3^-	F^-	Alk. [3]
Average of CO_2-rich water		12.8	6.05	310	1234	2.3	1345	−0.16	210.6	9.4	14.8	104.7	58.8	6.9	11.7	0.3	3.1	916
Standard deviation		3.9	0.32	53	466	1.1	555	0.24	199.4	9.8	16.6	84.0	20.4	6.3	5.8	0.9	3.0	383
Shallow groundwater																		
KW−16	Jul−01−98	20.2	6.56	379	125	5.8	86	−2.11	15.1	1.1	1.5	5.3	12.3	11.2	8.0	1.4	2.3	27
KW−16′	Feb−17−00	6.8	6.78	342	101	6.5	78	−2.51	9.8	0.6	2.4	5.4	11.0	14.8	11.6	4.1	0.3	18
KW−16″	Oct−16−00	22.0	6.13	317	268	7.5	181	−1.47	36.7	1.3	0.52	7.2	23.1	25.8	39.0	1.7	0.2	45
KW−17	Sep−05−00	25.7	6.75	405	234	6.0	208	−1.75	36.4	1.2	1.12	18.7	15.8	9.5	17.4	8.1	2.7	98
KW−18(a)	Jul−01−98	13.7	6.49	452	69	7.0	63	−2.09	6.0	0.7	1.6	3.7	19.4	4.8	1.4	0.4	0.4	24
KW−20(a)	Jul−07−99	17.1	6.27	378	35	6.3	39	−2.07	3.1	0.5	0.6	3.5	10.1	0.9	2.5	2.3	0.2	15
Average of shallow GW		17.6	6.50	379	139	6.5	109	−2.00	17.8	0.9	1.3	7.3	15.3	11.2	13.3	3.0	1.0	38
Standard deviation		6.1	0.24	43	85	0.6	63	0.32	13.7	0.3	0.6	5.2	4.7	7.9	12.7	2.5	1.1	28
Surface water																		
KW−5S	Jul−01−98	14.5	6.75	366	94	9.4	56	−2.35	6.9	1.7	1.4	3.7	7.5	3.7	3.4	2.4	0.5	24
KW−8S	Oct−30−98	13.4	7.77	354	53	9.4	52	−3.36	2.1	0.5	0.9	6.8	9.9	1.0	4.1	1.4	0.0	25
KW−9S	Oct−30−98	13.0	7.46	384	47	9.1	46	−3.16	3.3	0.6	0.7	5.1	10.1	1.2	4.3	1.4	0.1	19
KW−10S	Oct−30−98	10.2	6.86	389	60	9.6	50	−2.46	1.9	0.5	0.1	8.1	8.4	0.9	4.5	1.0	0.1	24
KW−13S	Aug−01−98	15.2	6.87	366	29	6.4	29	−2.89	1.8	0.4	0.6	3.3	6.4	0.7	2.2	4.2	0.1	9
KW−14S	Jul−01−99	17.2	6.89	358	46	8.7	54	−2.45	3.6	0.9	1.7	3.6	11.8	1.7	2.8	1.5	0.1	26
Average of surface water		13.9	7.10	370	55	8.8	48	−2.78	3.3	0.8	0.9	5.1	9.0	1.5	3.5	2.0	0.1	21
Standard deviation		2.1	0.38	13	20	1.1	9	0.38	1.8	0.5	0.5	1.8	1.8	1.0	0.8	1.1	0.1	6

[1] Data sources in parenthesis: "a" from Choi et al. [27], "b" from Choi et al. [26], and "c" from Choi et al. [25]. [2] Calculated from measured alkalinity and pH data using PHREEQC [36]. [3] Alkalinity as HCO_3^-.

Table 2. The concentrations of minor and trace elements in water samples in the Gangwon Province of South Korea. CO_2−rich water is grouped based on the Piper diagram (see Figure 3).

Sample No. (1)	Sampling Date	Concentrations (μg/L)											
		Fe	Sr	Mn	Al	Li	B	Cr	Zn	Rb	Cs	Ba	U
CO_2−rich water (Na−HCO_3 type)													
KW−1(a)	Sep−01−98	1465.0	284.1	294.0	961.0	254.0	104.0	24.0	15.7	666.0	18.1	218.0	2.6
KW−1′(a, c)	Jul−07−99	5220.0	412.0	103.0	270.0	50.9	16.4	5.7	8.4	121.0	22.4	214.0	3.9
KW−1″(b)	Apr−08−02	1215.0	337.5	133.0	457.5	107.2	69.6	2.1	26.6	178.4	17.4	188.4	3.9
KW−2(a)	Sep−01−98	2543.0	453.6	341.0	1270.0	345.0	123.0	24.8	44.2	932.0	25.1	282.0	25.1
KW−2′(a, c)	Jul−07−99	2123.0	524.0	113.0	117.0	61.9	22.9	10.7	8.3	150.0	24.9	170.0	25.0
KW−2‴(b)	Apr−08−02	6752.0	420.0	154.2	196.0	141.6	107.0	14.6	29.7	189.9	21.8	118.3	16.9
KW−2⁗(a)	Nov−19−10	6617.4	464.5	358.7	1517.4	607.1	146.6	n.d.	38.3	n.a.	n.a.	n.a.	n.a.
KW−3	Sep−01−98	3752.0	62.4	469.0	308.0	340.0	62.0	16.0	51.1	334.0	21.5	105.0	10.0
KW−3′	Jul−07−99	4125.0	53.0	127.0	53.5	93.1	12.7	4.9	23.2	54.0	21.0	53.4	6.9
KW−3‴(b, c)	Apr−08−02	3275.0	59.4	173.8	114.6	196.3	61.4	0.8	57.3	117.6	20.4	9.2	7.9
KW−4	Sep−01−98	1342.0	480.3	221.0	14.4	475.0	133.0	23.8	15.6	439.0	30.9	137.0	81.0
KW−4′	Jul−07−99	1794.0	495.0	95.4	3.1	220.0	37.4	8.0	12.9	80.8	30.0	105.0	56.5
KW−4‴(b, c)	Apr−08−02	1235.0	519.4	105.7	8.4	317.8	123.0	2.9	23.3	137.7	28.4	44.3	60.4
KW−4⁗	Nov−19−10	1824.8	476.1	260.4	n.d.	1336.2	138.1	n.d.	285.2	n.a.	n.a.	n.a.	n.a.
Average		3091.7	360.1	210.7	377.9	324.7	82.6	10.6	45.7	283.4	23.5	137.1	25.0
Std. Dev.		1872.7	169.9	112.8	484.4	320.4	46.3	8.8	68.1	258.2	4.2	77.2	25.3
CO_2−rich water (Ca−Na−HCO_3 type)													
KW−5	Jul−01−98	6267.0	1032.2	635.0	167.0	105.0	167.0	18.0	16.5	19.0	2.1	106.7	0.7
KW−5′	Jul−07−99	6702.0	1263.0	329.0	95.2	41.7	35.5	8.4	8.1	12.8	2.6	106.0	0.8
KW−5‴(b)	Apr−08−02	5758.0	1031.0	254.7	101.4	125.5	80.4	2.0	13.6	17.6	2.0	90.1	1.1
KW−5⁗	Nov−18−10	8987.0	1554.0	968.0	386.0	296.0	175.0	n.d.	n.d.	n.a.	n.a.	n.a.	n.a.
KW−7(b, c)	Apr−08−02	5653.0	1848.0	261.7	24.3	114.5	95.9	0.9	5.9	7.7	0.5	810.2	8.2
Average		6673.4	1345.6	489.7	154.8	136.5	110.8	5.9	8.8	14.3	1.8	278.2	2.7
Std. Dev		1216.4	316.2	276.7	124.1	84.9	53.1	6.7	5.8	4.4	0.8	307.2	3.2
CO_2−rich water (Ca−HCO_3 type)													
KW−8(b, c)	Oct−30−98	16309.0	1733.0	857.0	25.1	60.8	4.7	56.7	5.9	8.1	0.8	112.5	n.d.
KW−8′(a)	Nov−19−10	15620.2	1704.5	1353.6	n.d.	91.4	97.5	n.d.	55.8	n.a.	n.a.	n.a.	n.a.
KW−9(a, b, c)	Oct−30−98	6641.0	364.2	656.0	524.7	58.3	2.8	42.5	59.6	2.1	0.6	75.8	0.7
KW−10(a, b, c)	Oct−30−98	14335.0	492.6	676.0	480.5	82.2	2.2	47.3	10.6	13.1	3.7	96.9	n.d.
KW−10″(a)	Nov−19−10	29981.7	867.5	1235.5	723.7	123.5	153.6	n.d.	43.2	n.a.	n.a.	n.a.	n.a.

Table 2. *Cont.*

Sample No. [(1)]	Sampling Date	Concentrations (μg/L)											
		Fe	Sr	Mn	Al	Li	B	Cr	Zn	Rb	Cs	Ba	U
KW−11(c)	Apr−08−02	16256.0	1859.0	795.7	83.4	85.5	13.4	9.8	2.3	31.5	7.7	80.7	n.d.
KW−12	Jul−01−99	9225.0	1954.0	404.0	3.8	29.2	7.3	9.9	12.5	3.3	0.5	218.0	1.1
KW−12′(b, c)	Apr−08−02	8757.0	1848.0	293.1	13.9	117.8	12.7	1.9	20.3	4.1	0.4	243.2	1.2
KW−13	Aug−01−98	15231.0	1580.3	391.0	28.3	41.7	613.0	37.6	20.6	4.4	0.3	217.0	0.3
KW−13′	Jul−07−99	13812.0	1583.0	280.0	2.9	7.2	5.1	10.0	16.2	2.6	0.3	219.0	0.2
KW−14(c)	Jul−07−99	25516.0	752.0	259.0	5.6	12.2	3.9	8.0	62.3	11.5	1.0	273.0	n.d.
KW−14′(b)	Apr−08−02	24583.0	734.3	237.4	20.8	64.0	5.6	2.5	111.3	15.2	0.7	101.2	0.1
KW−15(c)	Oct−02−99	10932.0	1912.0	1416.0	95.7	147.0	15.6	0.5	6.2	6.9	0.2	85.3	0.2
Average		3091.7	360.1	210.7	377.9	324.7	82.6	10.6	45.7	283.4	23.5	137.1	25.0
Std. Dev.		1872.7	169.9	112.8	484.4	320.4	46.3	8.8	68.1	258.2	4.2	77.2	25.3
Shallow groundwater													
KW−16	Jul−01−98	6.3	31.1	0.9	6.7	5.7	5.5	0.3	22.0	1.7	n.d.	46.1	0.3
KW−16′	Feb−17−00	5.2	25.3	1.5	15.4	1.1	3.8	n.d.	42.1	1.1	n.d.	76.8	n.d.
KW−16″	Oct−16−00	25.3	63.4	1.3	71.9	130.9	21.1	0.7	3.3	1.1	0.2	1.8	6.4
KW−17	Sep−05−00	15.2	98.6	1.3	7.0	27.6	16.4	0.3	217.7	0.8	n.d.	2.4	3.4
KW−18(a)	Jul−01−98	6.7	63.0	3.4	4.0	0.9	1.9	2.7	7.1	n.d.	n.d.	44.2	n.d.
KW−20(a)	Jul−07−99	23.0	24.0	1.2	17.0	n.d.	4.6	0.6	12.9	1.9	n.d.	38.4	0.3
Average		13.6	50.9	1.6	20.3	27.7	8.9	0.8	50.8	1.1	0.1	34.9	1.7
Std. Dev.		8.2	26.9	0.8	23.5	47.1	7.2	0.9	75.7	0.6	0.0	26.2	2.4
Surface water													
KW−5S	Jul−01−98	67.3	38.7	16.9	53.6	0.9	19.5	2.1	5.9	3.0	n.d.	36.4	n.d.
KW−8S	Oct−30−98	34.3	35.6	1.8	1.3	0.5	n.d.	4.3	0.8	0.8	n.d.	44.1	n.a.
KW−9S	Oct−30−98	33.5	36.4	10.9	2.6	3.0	n.d.	4.1	1.3	0.9	n.d.	63.7	0.7
KW−10S	Oct−30−98	61.2	36.2	3.7	6.0	1.4	n.d.	6.9	1.1	1.1	n.d.	38.3	n.d.
KW−13S	Aug−01−98	35.2	20.8	1.5	14.4	0.2	33.8	3.1	2.6	0.9	n.d.	31.6	n.a.
KW−14S	Jul−01−99	91.0	32.0	2.2	4.7	n.d.	2.6	0.9	1.4	2.0	n.d.	106.0	n.d.
Average		53.8	33.3	6.2	13.8	1.0	9.3	3.6	2.2	1.4	–	53.4	–
Std. Dev.		21.4	5.9	5.8	18.3	1.0	13.0	1.9	1.8	0.8	–	25.7	–
Guidelines for Drinking−Water Quality in Chemical Aspects (WHO)		–	–	–	–	–	2400	50	–	–	–	1300	30
Guidelines for Drinking−Water Quality in Acceptability Aspects (WHO)		300	–	100	100	–	–	–	4000	–	–	–	–

Abbreviations: n.a. = not analyzed, n.d. = not detected, Std. Dev. = Standard deviation. [(1)] Data sources in parenthesis: "a" for Fe by Choi et al. [27]; "d" for data of Fe, Sr, Mn and Al by Choi et al. [26]; and "c" for data of Fe and Al by Choi et al. [25].

Table 3. Isotopic compositions of water samples in the Gangwon Province of South Korea. CO_2−rich water is grouped based on the Piper diagram (see Figure 3).

Sample no. [(1)]	Sampling Date	$\delta^{18}O$ (‰)	δD (‰)	$\delta^{13}C$ (‰)	Tritium (T.U.)
CO_2−rich water (Na−HCO_3 type)					
KW−1 (a)	Sep−01−98	−10.9	−76.8	−8.1	5.0
KW−1′ (a)	Jul−07−99	−11.3	−81.6	−4.0	n.a.
KW−2 (a)	Sep−01−98	−11.7	−83.3	−8.3	1.7
KW−2′ (a)	Jul−07−99	−12.1	−89.3	−0.3	n.a.
KW−2′′′′ (a)	Nov−19−10	−11.8	−82.5	−3.7	n.a.
KW−3	Sep−01−98	−11.3	−78.3	−7.8	0.0
KW−3′	Jul−07−99	−11.3	−83.3	−2.8	n.a.
KW−4	Sep−01−98	−11.5	−80.0	−3.0	0.0
KW−4′	Jul−07−99	−11.4	−84.0	−7.4	n.a.
KW−4′′′′	Nov−19−10	−11.3	−80.1	−4.5	n.a.
CO_2−rich water (Ca−Na−HCO_3 type)					
KW−5	Jul−01−98	−10.4	−72.7	−8.8	7.6
KW−5′	Jul−07−99	−10.5	−75.3	−5.3	n.a.
KW−5′′′′	Nov−18−10	−10.6	−72.7	−4.6	n.a.
CO_2−rich water (Ca−HCO_3 type)					
KW−8 (a)	Oct−30−98	−10.7	−74.4	0.8	2.5
KW−8′ (a)	Nov−19−10	−10.7	−73.6	−4.3	n.a.
KW−9	Oct−30−98	−10.1	−72.3	−6.1	7.6
KW−10	Oct−30−98	−10.8	−75.2	−5.1	5.2
KW−10″ (a)	Nov−19−10	−10.7	−74.7	−4.7	n.a.
KW−12	Aug−01−98	−10.6	−77.7	−5.4	7.0
KW−13	Aug−01−98	−10.7	−69.5	n.a.	7.0
KW−13′	Jul−07−99	−10.7	−77.3	n.a.	n.a.
KW−14	Jul−07−99	−9.9	−70.3	−6.6	n.a.
KW−15	Sep−30−99	n.a.	n.a.	−4.7	n.a.
Shallow groundwater					
KW−16	Jul−01−98	−8.6	−54.8	−16.8	4.1
KW−16′	Feb−17−00	−8.7	−62.3	−15.7	6.7
KW−18 (a)	Jul−01−98	−8.9	−58.3	−19.0	6.1
KW−20 (a)	Jul−07−99	−11.0	−81.3	−17.2	n.a.
Surface water					
KW−5S	Oct−30−98	−10.2	−72.4	n.a.	7.9
KW−8S	Jul−01−98	−8.7	−65.2	n.a.	12.5

n.a.: not analyzed. [(1)] Data of the samples with "a" in parenthesis are from Choi et al. [27].

Table 4. Chemical compositions of rock samples collected from the vicinity of CO_2−rich water in the Gangwon Province of South Korea.

Rock Type [(1)]	Sample No.	SiO_2	Al_2O_3	Fe_2O_3	MnO	CaO	MgO	K_2O	Na_2O	P_2O_5	TiO_2	Loss−on−Ignition	Sum
		wt. %											
Na−HCO$_3$ type													
Biotite granite	KW−1	74.68	13.85	1.33	0.11	0.52	0.12	4.20	3.14	0.03	0.03	0.55	98.56
Biotite granite (a)	"	73.83	13.99	1.67	0.05	0.96	0.40	4.99	2.83	0.04	0.17	0.54	99.47
Biotite granite gneiss	"	73.43	13.99	2.04	0.05	0.83	0.19	5.48	3.21	0.03	0.19	0.27	99.71
Porphyroblastic gneiss	"	71.16	15.16	2.15	0.04	1.23	0.24	5.55	3.50	0.04	0.22	0.29	99.58
Biotite granite (a)	KW−2	73.17	14.30	1.94	0.08	1.75	0.30	4.04	3.14	0.06	0.23	0.34	99.35
Granite gneiss	KW−3	74.91	14.21	1.55	0.06	1.25	0.15	4.24	3.06	0.02	0.06	0.39	99.90
Biotite granite gneiss	KW−4	68.93	15.47	3.40	0.06	3.19	1.33	2.66	3.19	0.12	0.33	0.47	99.15
Biotite granite	"	76.65	12.45	1.33	0.03	0.43	0.02	4.53	3.53	–	0.04	0.29	99.30
Porphyroblastic gneiss	"	63.39	17.16	5.11	0.10	3.91	2.35	3.15	3.23	0.15	0.63	1.29	100.47
Average		72.24	14.51	2.28	0.06	1.56	0.57	4.32	3.20	0.06	0.21	0.49	99.50
Ca−HCO$_3$ type													
Biotite granite gneiss	KW−8	73.90	14.81	1.43	0.02	0.97	0.29	4.69	3.02	0.05	0.19	0.69	100.06
Biotite granite (a)	"	69.47	15.64	3.45	0.06	2.90	1.13	4.06	2.76	0.11	0.47	0.42	100.47
Biotite granite (a)	"	72.40	14.70	2.33	0.04	2.08	0.63	4.03	2.89	0.09	0.32	0.48	99.99
Biotite granite (a)	"	67.96	15.93	4.15	0.06	3.28	1.38	3.43	2.88	0.13	0.56	0.35	100.11
Biotite granite (a)	KW−9	67.48	15.95	3.52	0.06	3.42	1.09	3.89	2.88	0.11	0.44	0.60	99.44
Banded gneiss	KW−11	70.59	15.67	3.01	0.04	1.97	0.98	4.02	2.76	0.10	0.40	1.05	100.59
Banded gneiss	KW−12	75.20	12.44	4.06	0.08	1.26	1.31	2.24	2.35	0.04	0.31	0.83	100.12
Average		71.00	15.02	3.14	0.05	2.27	0.97	3.77	2.79	0.09	0.38	0.63	100.11

[(1)] Data of the samples denoted with "a" in parenthesis are from Choi et al. [27].

4. Results and Discussion

4.1. Hydrochemical and Isotopic Data

Data on field measurements and major constituents of water samples are summarized in Table 1. The concentrations of minor to trace elements are shown in Table 2. It is notable that the CO_2-rich water samples show relatively low pH values (5.5 to 6.7) and high EC values (454 to 2220 μS/cm), while the shallow groundwater and surface water have higher pH values (averages of 6.5 and 7.1, respectively) and lower EC values (averages of 138.7 and 54.8 μS/cm, respectively) than the CO_2-rich water (see Table 1). The P_{CO2} values of the CO_2-rich water range from $10^{-0.66}$ to $10^{+0.41}$ atm, and are clearly distinguished from those of shallow groundwater (average of 10^{-2} atm) and surface water (average of $10^{-2.8}$ atm) (Table 1).

4.1.1. Origin of the CO_2

The relation between P_{CO2} and $\delta^{13}C$ of water samples in Figure 2 shows a clear difference between CO_2-rich water and the others. The CO_2-rich water has heavy $\delta^{13}C$ values (average = –4.9‰; Table 3) as well as elevated P_{CO2} (average = $10^{-0.13}$ atm), whereas the shallow groundwater and surface water show considerably lighter $\delta^{13}C$ values as well as lower P_{CO2}. Considering the high $\delta^{13}C$ values and the few carbonate minerals in the study area, external CO_2 seems a likely major source for the high P_{CO2} rather than in-situ reactions such as the decomposition of organic matter or the dissolution of carbonate minerals.

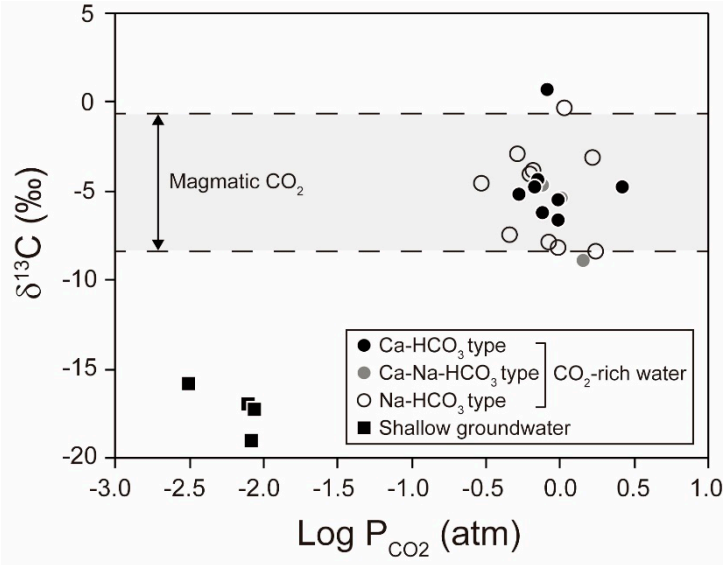

Figure 2. Plots of log P_{CO2} versus $\delta^{13}C$ values for water samples from the Gangwon Province of South Korea. The water types were classified based on the Piper diagram (see below). The sources of data used are shown in Tables 1 and 3.

Potential external CO_2 sources include diagenetic and metamorphic reactions [38–40] and deep-seated mantle and magmatic CO_2. However, the diagenetic and metamorphic reactions can be excluded, because burial and/or heating had not been observed to acquire a temperature above 450 °C in the study area based on its sedimentary sequence [39,41,42]. Moreover, the $\delta^{13}C$ values of the CO_2-rich water (–8.8 to 0.8‰) are in good agreement with the general $\delta^{13}C$ range of the magmatic CO_2 (–8 to –1‰) and smaller than that of the metamorphic CO_2 (0 to +10‰) [43,44]. Based on these facts, magmatic CO_2 gas seems a major source for the elevated P_{CO2} in the CO_2-rich water of this study. Similarly, previous studies suggested that the CO_2 gas comes from deep-seated sources such as magmatic CO_2 based on $\delta^{13}C$ data in the study area [25,27].

4.1.2. Three Water Types of CO_2-Rich Water

The hydrochemical compositions of water samples were plotted on a Piper diagram to classify water types and to understand the hydrochemical characteristics of each water type (Figure 3). The CO_2-rich water in the study area is clearly grouped into three water types, similar to the previous studies [25–27]. The three types of Na-HCO_3, Ca-Na-HCO_3 and Ca-HCO_3 are distinct from each other based on the major cations, i.e., Ca and Na + K, while all have a high HCO_3 ratio compared to the surface water and shallow groundwater in the Piper diagram (Figure 3).

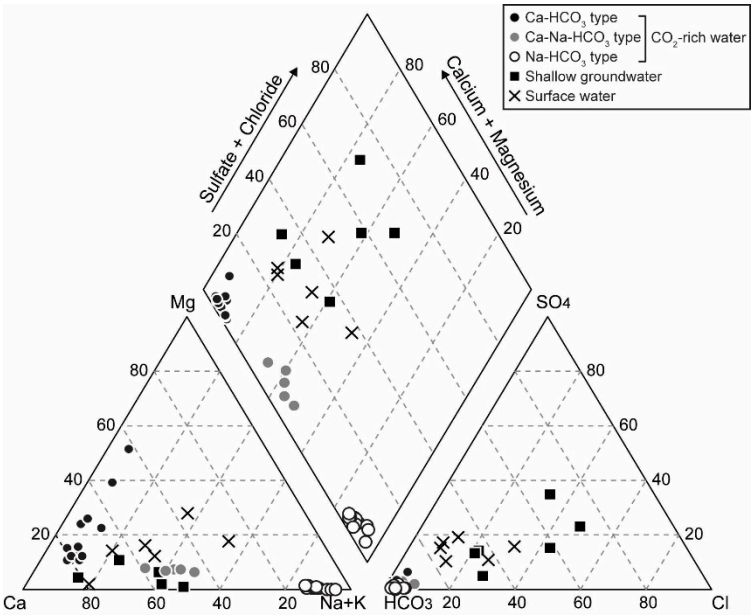

Figure 3. Piper diagram showing the hydrochemical compositions of water samples in the study area. CO_2−rich water in the Gangwon area is clearly grouped into three water types, Na–HCO_3, Ca−Na−HCO_3 and Ca−HCO_3.

The three types of CO_2−rich water differ in terms of trace element concentrations as well as major ions, and their correlations with total dissolved solids (TDS) (Figures 4 and 5). In particular, the Na−HCO_3 and Ca−HCO_3 types are distinct from each other by Na, Ca, K, Mg, F and SiO_2, while the Ca−Na−HCO_3 type has an intermediate characteristic between the other two water types (Figure 4). All the types of CO_2−rich water contain high concentrations of trace elements such as Fe, Mn, Sr, Li, Rb and Cs compared to the surface water and shallow groundwater (Table 2 and Figure 5). However, Fe concentrations are generally higher in the Ca−HCO_3 type (up to 26 mg/L) than those in the Na−HCO_3 type (Figure 5a). Mn and Sr concentrations are high in the Ca–HCO_3 type (Figure 5b,c), while Li, Rb and Cs, which are chemically compatible with Na and K, are enriched in the Na−HCO_3 type (Figure 5d−f).

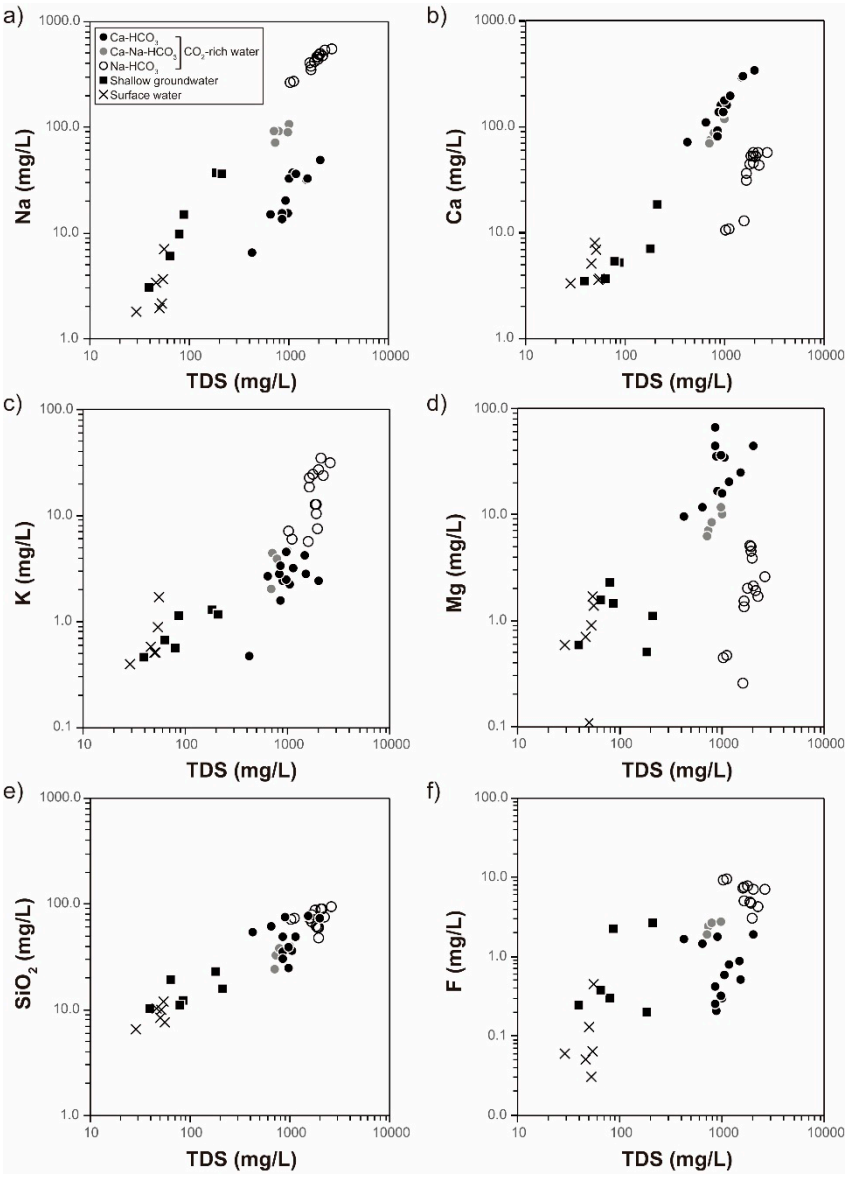

Figure 4. Plots of TDS versus major elements for water samples: (**a**) Na, (**b**) Ca, (**c**) K, (**d**) Mg, (**e**) SiO_2 and (**f**) F.

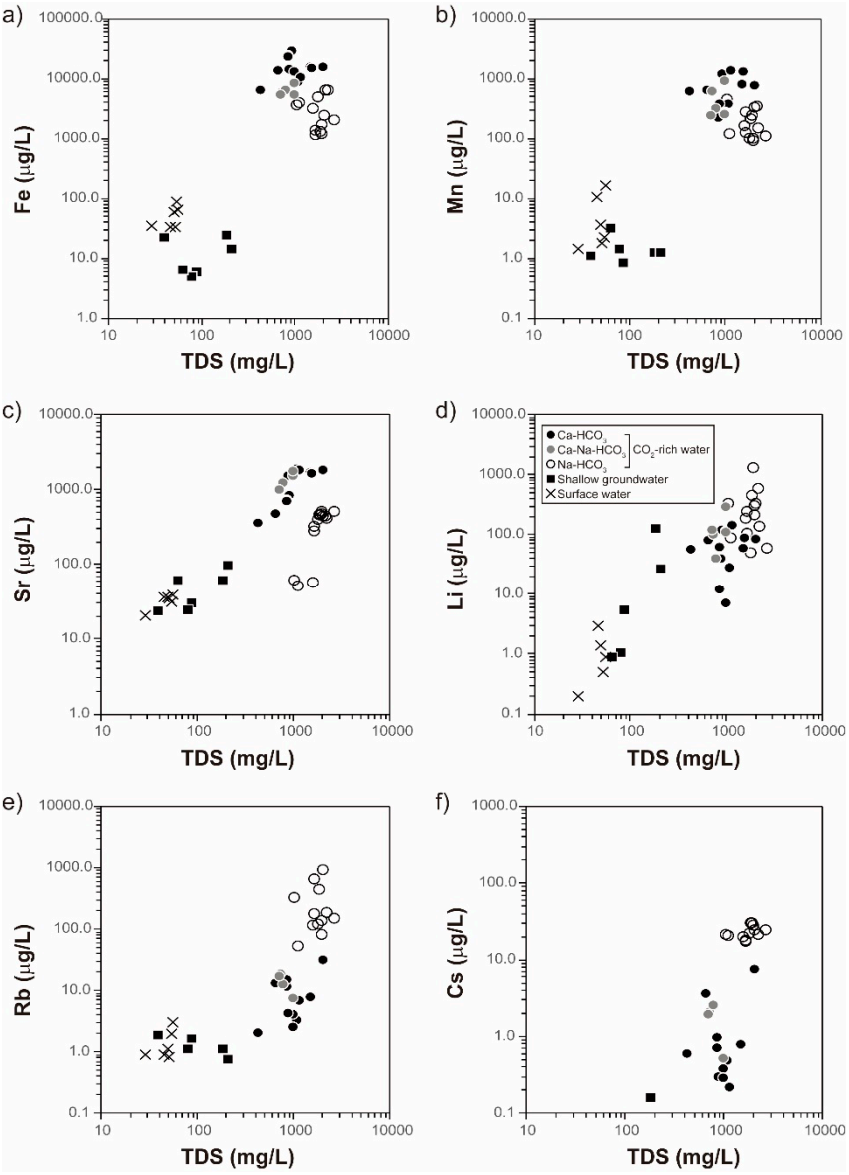

Figure 5. Plots of TDS versus trace elements for water samples: (**a**) Fe, (**b**) Mn, (**c**) Sr, (**d**) Li, (**e**) Rb and (**f**) Cs.

4.1.3. Evolutionary Processes for Each Water Type of CO_2−Rich Water

The different distribution patterns of major and minor elements depending on the water type in Figures 4 and 5 indicate that each type of CO_2−rich water may follow a different geochemical process. Moreover, the chemical compositions of rock samples collected from the vicinity of the CO_2−rich water show no remarkable differences (Table 4). The only noticeable difference is the Na_2O content (p−value of the Mann−Whitney U−test = 0.002). Thus, the geology does not seem to be a major factor in differentiating the hydrochemistry in the CO_2−rich water, and circulation depths and residence times are examined for each water type below.

The circulation depth and residence time of water can be estimated using water isotope ratios ($\delta^{18}O$ and δD) and tritium concentrations (e.g., [43]). All $\delta^{18}O$ and δD values of the water samples from the study area are plotted close to the global meteoric water line (GMWL), suggesting that all the water is of meteoric origin (Figure 6a and Table 3). However, the Ca−HCO_3 type CO_2−rich water has a heavier isotopic composition than the Na−HCO_3 type, whose ^{18}O and δD are relatively depleted compared to the other water types. This suggests that the Na−HCO_3 type CO_2−rich water was

recharged at a relatively high altitude and circulated through a deep path for a relatively long residence time in the subsurface [25,27]. In the diagram of tritium concentrations versus $\delta^{18}O$ values (Figure 6b), the Na−HCO_3 type CO_2−rich water also has lower tritium contents than the other types, indicating older age. Meanwhile, the Ca−HCO_3 type CO_2−rich water has tritium concentrations similar to or higher than the shallow groundwater and surface water. This different tritium content suggests that the Na−HCO_3 type has been little affected by the surface water and the shallow groundwater after the intensive water−rock interaction until discharge. On the other hand, the Ca−HCO_3 type reflects a relatively low extent of water–rock reactions and mixing with recently recharged water [27].

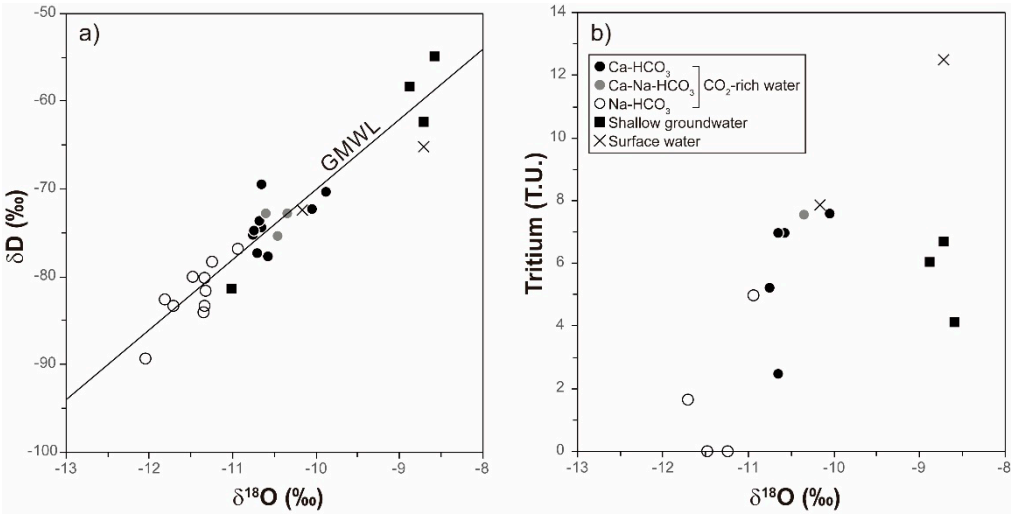

Figure 6. (**a**) Diagram of $\delta^{18}O$ versus δD values. The solid line is the global meteoric water line (δD = 8 × $\delta^{18}O$ + 10). (**b**) Diagram of tritium versus $\delta^{18}O$.

The study results are consistent with the previous results on the genesis and evolution of CO_2−rich water in the study area [25–27]. In the previous studies, the Na−HCO_3 type CO_2−rich water was explained by the water−rock interaction caused by the deep−seated CO_2, which was enhanced by high reservoir temperatures around 140–160 °C [25]. The mixing of the Na−HCO_3 type water with shallow groundwater would result in successive changes of groundwater chemistry from the Ca−Na−HCO_3 type into the Ca−HCO_3 type [26].

The Ca−HCO_3 type and Na−HCO_3 type have gone through different reaction times and circulation depths, while the Ca−Na−HCO_3 type has intermediate characteristics between the other two types. It can be suggested that the supply of gaseous CO_2 and the subsequent CO_2−water−rock interaction for a long residence time at a deep depth causes the Na−HCO_3 type CO_2−rich water, while the vertical migration of CO_2−rich fluid containing high concentrations of chemical species into shallow aquifers causes the Ca−HCO_3 type CO_2−rich water.

4.2. Behaviors of Trace Elements during Different Evolutional Processes

The hydrochemical characteristics of CO_2−rich water were scrutinized by PCA using 21 chemical species (Na, K, Mg, Ca, SiO_2, Cl, SO_4, F, Fe, Sr, Mn, Al, Li, B, Cr, Zn, Rb, Cs, Ba, U and alkalinity), four measured variables (pH, Eh, EC, DO), and two calculated variables (P_{CO2} and TDS) to identify major evolutionary processes for each water type. As a result, the surface water and shallow groundwater and the three types of CO_2−rich water are distinctly clustered by the first two components, as shown in Figure 7a.

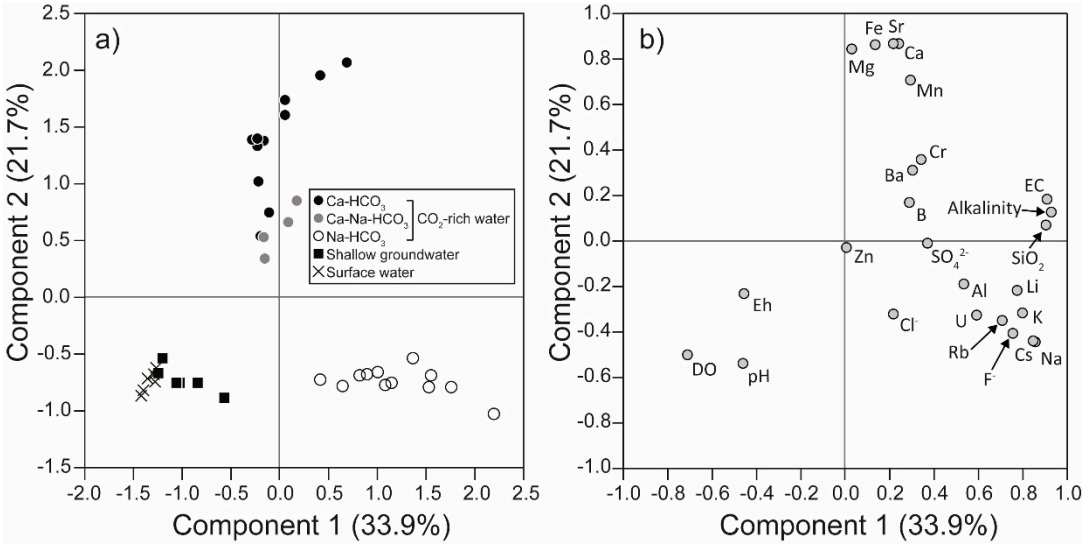

Figure 7. The first two components, 1 and 2, obtained by principal component analysis (PCA): (**a**) Scores of water samples, (**b**) Loadings of variables.

The CO_2−rich water is clearly distinguished from both the surface water and the shallow groundwater by component 1, while the three types of CO_2−rich water are made distinct by component 2. Component 1 has negative relations with DO, Eh, and pH, whose high values indicate recent recharge, while component 1 has positive correlations with P_{CO2}, EC, alkalinity, SiO_2, and TDS. Thus, it can be concluded that component 1 represents that the CO_2−rich water is influenced by the CO_2 supply and the subsequent CO_2−water−rock interaction in the study area. In contrast, component 2 indicates that the three types of CO_2−rich water have different relationships with trace elements, which are discussed below in relation to the major geochemical process.

4.2.1. Extensive Water−Rock Interactions in the Na−HCO_3 Type

The Na−HCO_3 type CO_2−rich water shows a significant relation with alkali metals such as Li, Rb and Cs as well as Na and K, and also a strong relationship with Al, F, and U (Figure 7b), which suggests that the high concentrations of trace elements in the Na−HCO_3 type CO_2−rich water may be attributed to extensive water−rock interactions.

Specifically, fluoride is a well-known indicator of water−rock interactions in silicate bedrock [45], and the high F concentrations of the Na−HCO_3 type CO_2−rich water imply extensive water−rock interaction. The concentration of uranium also indicates that the Na−HCO_3 type CO_2−rich water has undergone more water−rock interactions than the Ca−HCO_3 type because the only source of U is the geology in the study area, but there is no difference in the rock compositions near the two types of CO_2−rich water (Figure 1 and Table 4). In general, U is dominantly present as uranyl (UO_2^{2+}) in oxic and suboxic conditions, and the uranyl forms uranyl carbonate ($UO_2(CO_3)_2^{2-}$ or $UO_2(CO_3)_3^{4-}$) when the bicarbonate concentration is high, as in the CO_2−rich water. In addition, it is known that U mobility is enhanced when the Ca concentration is high because the formation of calcium uranyl carbonate complexes (e.g., $Ca_2UO_2(CO_3)_3$) inhibits the sorption of U to the mineral surface [46–51]. For this reason, high uranium concentrations have often been observed in the Ca−HCO_3 type groundwater [48,50,51]. However, in this study, uranium shows a positive correlation with the Na−HCO_3 type CO_2−rich water (Figure 7), and U concentrations are higher in the Na−HCO_3 type than in the Ca−HCO_3 type (Table 2).

4.2.2. Mixing and Cation Exchange in the Ca−HCO_3 Type

The Ca−HCO_3 type CO_2−rich water is clearly differentiated from both the Na−HCO_3 type CO_2−rich water and the shallow groundwater by component 2 and is highly correlated with Ca, Mg, Sr, Fe, and Mn (Figure 7). This indicates that the Ca−HCO_3 type CO_2−rich water is formed by

the mixing of shallow groundwater and the Na−HCO_3 type CO_2−rich water, and then affected by other geochemical processes such as cation exchanges.

In particular, high Fe and Mn concentrations seem to be derived from the reverse cation exchange, similar to Ca and Mg as described by [27], for the following reasons. First, sulfide minerals such as pyrite (FeS_2) are not found in the bedrock of the study area (see Figure 1), and the average sulfate concentration of the Ca−HCO_3 type CO_2−rich water is low (11.2 mg/L). Thus, Fe and Mn concentrations did not increase due to the dissolution of sulfide minerals. Second, the Fe and Mn concentrations of the Na−HCO_3 type CO_2−rich water are lower than those of the Ca−HCO_3 type CO_2−rich water (Table 2 and Figure 5), and thus the concentrations of Fe and Mn in the Ca−HCO_3 type CO_2−rich water were not increased by the inflow of deep groundwater such as the Na−HCO_3 type CO_2−rich water. A previous study suggested that reverse cation exchange during the mixing of Na−HCO_3 type CO_2−rich water with shallow groundwater results in the Ca−HCO_3 type CO_2−rich water in the study area [27].

4.3. Comparison with WHO Guidelines for Drinking−Water Quality

The study results indicate that the dissolution of gaseous CO_2 and/or the inflow of CO_2−rich fluid into aquifers can degrade groundwater quality by increasing the concentrations of chemical species. To evaluate the impact of these CO_2−triggered geochemical processes (i.e., water−rock interactions and cation exchanges) on groundwater quality, the levels of trace elements were compared to those in the guidelines for drinking−water quality of the World Health Organization (WHO) (Table 2) [52]. The WHO suggests the guideline values of contaminants in drinking water as the guidelines for drinking−water quality. The guidelines were established for toxic contaminants that are harmful to human health, including B, Cr, Ba, and U in Table 2 (chemical aspects), and for contaminants regarding public acceptability in taste, odor and appearance (acceptability aspects), including Fe, Mn, Al, and Zn as in Table 2.

In all types of CO_2−rich water, the trace elements in chemical aspects (i.e., B, Cr, Ba, and U) do not exceed the guideline values. However, among the elements in acceptability aspects (i.e., Fe, Mn, Al and Zn), Fe and Mn significantly exceed the guideline levels: 10.9 and 2.1 times in the Na−HCO_3 type, 22.2 and 4.9 times in the Ca−Na−HCO_3 type, and 53.1 and 6.8 times in the Ca−HCO_3 type, respectively. In addition, Al is about four times as high as the guideline level in the Na−HCO_3 type, probably because of extensive water−rock interactions in deep and high−temperature conditions. Although uranium (U) does not exceed the guideline in all types of CO_2−rich water, the average concentration of U is close to the guideline (30 μg/L) in the Na−HCO_3 type CO_2−rich water (25.02 μg/L), and the three samples of the Na−HCO_3 type (KW−4 in Table 2) show U concentrations exceeding the guideline.

The high concentrations of Fe, Mn and Al can be harmful to human health when the water is taken for a long time [52]. In addition, when the groundwater is exposed to an oxic environment, they are rapidly oxidized to produce oxides/hydroxides, causing discoloration and increasing the turbidity of water [52,53]. Meanwhile, the long−term exposure to high concentrations of uranium is known to increase the incidence of cancer as well as kidney damage [52]. These results indicate that the long−term leakage of CO_2 in silicate bedrock areas such as granite and gneiss may significantly increase the risk to human health due to increased trace elements [30].

5. Summary and Conclusions

To evaluate the potential impact of CO_2 gas and CO_2−rich fluid leaked from GCS sites on groundwater quality, we investigated the hydrochemical and isotopic characteristics of naturally occurring CO_2−rich water and compared them with those of the adjacent shallow groundwater and surface water. The CO_2−rich water showed low pH, high P_{CO2}, and high TDS including major and minor elements compared to the shallow groundwater and the surface water. The $\delta^{13}C$ values of CO_2−rich water indicated that the deep−seated magmatic CO_2 caused the elevated P_{CO2} values in the CO_2−rich water.

The CO_2−rich water in the study area was divided into three types, Na−HCO_3, Ca−HCO_3 and Ca−Na−HCO_3, based on the hydrochemical compositions. Since the geochemical compositions of rock samples obtained in the vicinity of CO_2−rich water did not show any remarkable differences regardless of water type, the water types were ascribed to geochemical evolutionary processes. The water isotope ratios, tritium concentrations, and hydrochemical species suggested that the Na−HCO_3 type CO_2−rich water had been formed through extensive CO_2−water−rock interactions for a relatively long residence time at a deep depth, but was rarely affected by shallow aquifers until discharge, while the Ca−HCO_3 type CO_2−rich water reflected a relatively low extent of water−rock reactions and mixing with recently recharged water.

Specifically, the leakage of gaseous CO_2 into the groundwater aquifer at a deep depth seemed to enhance water−rock interactions, which consequently increased the concentrations of trace elements such as Li, Rb, Cs, Al and U in the Na−HCO_3 type CO_2−rich water. Then the migration of this high TDS CO_2−rich fluid into shallow aquifers and the following geochemical processes such as mixing and cation exchange increased metal concentrations such as Sr, Fe, and Mn. As a result, the concentrations of Fe, Mn, and Al in CO_2−rich water exceeded the guideline levels of the WHO. Although not exceeding the drinking water standard, elevated U concentrations in the Na−HCO_3 CO_2−rich water implied an increased risk to human health by the mobilization of U due to extensive CO_2−water−rock interactions.

The study results imply that the potential impact of CO_2 leakage on groundwater quality depends on the geochemical evolutionary processes of leaked CO_2 (e.g., reaction time and depth). In addition, changes in the hydrochemistry of groundwater due to the CO_2 leakage are related to groundwater contamination, especially increased trace elements such as iron, manganese, aluminum, and uranium in silicate basement areas.

Author Contributions: The authors have contributed to this work as follows: conceptualization, S.-T.Y. and H.-K.D.; methodology, H.-K.D., Y.-G.R., and S.-T.Y.; formal analysis, H.-K.D., Y.-G.R., and H.-S.C.; investigation, H.-K.D. and H.-S.C.; writing—original draft preparation, H.-K.D. and Y.-G.R.; writing—review and editing, S.Y. and S.-T.Y.; supervision, S.-T.Y.; project administration, S.-T.Y.; funding acquisition, S.-T.Y. All authors have read and agreed to the published version of the manuscript.

Funding: This research was funded by the Korea Ministry of Environment as "CO_2 Storage Environmental Management (K−COSEM) Research Center Research Program, grant number 2014001810001" and partly by the 2010 Eco−Technopia 21 Project for early−stage field campaigns.

Conflicts of Interest: The authors declare no conflict of interest.

References

1. Bachu, S.; Bennion, D.B. Experimental assessment of brine and/or CO2 leakage through well cements at reservoir conditions. *Int. J. Greenh. Gas Control* **2009**, *3*, 494–501. [CrossRef]
2. Harvey, O.R.; Qafoku, N.P.; Cantrell, K.J.; Lee, G.; Amonette, J.E.; Brown, C.F. Response to Comment on "Geochemical Implications of Gas Leakage associated with Geologic CO2 Storage—A Qualitative Review". *Environ. Sci. Technol.* **2013**, *47*, 4951–4952. [CrossRef]
3. Lemieux, J.-M. Review: The potential impact of underground geological storage of carbon dioxide in deep saline aquifers on shallow groundwater resources. *Hydrogeol. J.* **2011**, *19*, 757–778. [CrossRef]
4. Metz, B.; Davidson, O.; De Coninck, H.C.; Loos, M.; Meyer, L.A. *IPCC, 2005: IPCC Special Report on Carbon Dioxide Capture and Storage*; Working Group III of the Intergovernmental Panel on Climate Change: Cambridge, UK; New York, NY, USA, 2005; p. 442.
5. Pruess, K. On CO2 fluid flow and heat transfer behavior in the subsurface, following leakage from a geologic storage reservoir. *Environ. Earth Sci.* **2007**, *54*, 1677–1686. [CrossRef]
6. Benson, S.M.; Cole, D.R. CO2 Sequestration in Deep Sedimentary Formations. *Elements* **2008**, *4*, 325–331. [CrossRef]
7. DOEFE (USDOE Office of Fossil Energy (FE) (United States)). *Report of the Interagency Task Force on Carbon Capture and Storage*; DOEFE: Washington, DC, USA, 2010.

8. Keating, E.; Fessenden, J.; Kanjorski, N.; Koning, D.J.; Pawar, R. The impact of CO2 on shallow groundwater chemistry: Observations at a natural analog site and implications for carbon sequestration. *Environ. Earth Sci.* **2009**, *60*, 521–536. [CrossRef]
9. Kharaka, Y.K.; Thordsen, J.J.; Kakouros, E.; Ambats, G.; Herkelrath, W.N.; Beers, S.R.; Birkholzer, J.; Apps, J.A.; Spycher, N.F.; Zheng, L.; et al. Changes in the chemistry of shallow groundwater related to the 2008 injection of CO2 at the ZERT field site, Bozeman, Montana. *Environ. Earth Sci.* **2009**, *60*, 273–284. [CrossRef]
10. Mickler, P.J.; Yang, C.; Scanlon, B.R.; Reedy, R.; Lu, J. Potential Impacts of CO2Leakage on Groundwater Chemistry from Laboratory Batch Experiments and Field Push–pull Tests. *Environ. Sci. Technol.* **2013**, *47*, 10694–10702. [CrossRef]
11. Trautz, R.C.; Pugh, J.D.; Varadharajan, C.; Zheng, L.; Bianchi, M.; Nico, P.S.; Spycher, N.F.; Newell, D.; Esposito, R.A.; Wu, Y.; et al. Effect of Dissolved CO2on a Shallow Groundwater System: A Controlled Release Field Experiment. *Environ. Sci. Technol.* **2012**, *47*, 298–305. [CrossRef]
12. Humez, P.; Lions, J.; Negrel, P.; Lagneau, V. CO2 intrusion in freshwater aquifers: Review of geochemical tracers and monitoring tools, classical uses and innovative approaches. *Appl. Geochem.* **2014**, *46*, 95–108. [CrossRef]
13. Newell, D.; Larson, T.; Perkins, G.; Pugh, J.; Stewart, B.; Capo, R.; Trautz, R. Tracing CO2 leakage into groundwater using carbon and strontium isotopes during a controlled CO2 release field test. *Int. J. Greenh. Gas Control* **2014**, *29*, 200–208. [CrossRef]
14. Schulz, A.; Vogt, C.; Lamert, H.; Peter, A.; Heinrich, B.; Dahmke, A.; Richnow, H.-H. Monitoring of a Simulated CO2Leakage in a Shallow Aquifer Using Stable Carbon Isotopes. *Environ. Sci. Technol.* **2012**, *46*, 11243–11250. [CrossRef]
15. Choi, H.; Woo, N.C. Natural analogue monitoring to estimate the hydrochemical change of groundwater by the carbonating process from the introduction of CO2. *J. Hydrol.* **2018**, *562*, 318–334. [CrossRef]
16. Navarre-Sitchler, A.K.; Maxwell, R.M.; Siirila-Woodburn, E.R.; Hammond, G.E.; Lichtner, P.C. Elucidating geochemical response of shallow heterogeneous aquifers to CO2 leakage using high-performance computing: Implications for monitoring of CO2 sequestration. *Adv. Water Resour.* **2013**, *53*, 45–55. [CrossRef]
17. Yang, Q.; Matter, J.; Stute, M.; Takahashi, T.; O'Mullan, G.; Umemoto, K.; Clauson, K.; Dueker, M.E.; Zakharova, N.V.; Goddard, J.; et al. Groundwater hydrogeochemistry in injection experiments simulating CO2 leakage from geological storage reservoir. *Int. J. Greenh. Gas Control* **2014**, *26*, 193–203. [CrossRef]
18. Humez, P.; Lagneau, V.; Lions, J.; Negrel, P. Assessing the potential consequences of CO2 leakage to freshwater resources: A batch-reaction experiment towards an isotopic tracing tool. *Appl. Geochem.* **2013**, *30*, 178–190. [CrossRef]
19. Lu, J.; Partin, J.W.; Hovorka, S.D.; Wong, C. Potential risks to freshwater resources as a result of leakage from CO2 geological storage: A batch-reaction experiment. *Environ. Earth Sci.* **2009**, *60*, 335–348. [CrossRef]
20. Ju, Y.; Beaubien, S.E.; Lee, S.-S.; Kaown, D.; Hahm, D.; Lee, S.; Park, I.-W.; Park, K.; Yun, S.-T.; Lee, K.-K. Application of natural and artificial tracers to constrain CO2 leakage and degassing in the K-COSEM site, South Korea. *Int. J. Greenh. Gas Control* **2019**, *86*, 211–225. [CrossRef]
21. Cahill, A.G.; Marker, P.; Jakobsen, R. Hydrogeochemical and mineralogical effects of sustained CO2contamination in a shallow sandy aquifer: A field-scale controlled release experiment. *Water Resour. Res.* **2014**, *50*, 1735–1755. [CrossRef]
22. Roberts, J.J.; Wilkinson, M.; Naylor, M.; Shipton, Z.K.; Wood, R.A.; Haszeldine, R.S. Natural CO2sites in Italy show the importance of overburden geopressure, fractures and faults for CO2storage performance and risk management. *Geol. Soc. Spéc.* **2017**, *458*, 181–211. [CrossRef]
23. Chae, G.; Yu, S.; Jo, M.; Choi, B.-Y.; Kim, T.; Koh, D.-C.; Yun, Y.-Y.; Yun, S.-T.; Kim, J.-C. Monitoring of CO2-rich waters with low pH and low EC: An analogue study of CO2 leakage into shallow aquifers. *Environ. Earth Sci.* **2016**, *75*, 1–15. [CrossRef]
24. Menció, A.; Guasch, H.; Soler, D.; Canelles, A.; Zamorano, M.; Brusi, D. Influence of regional hydrogeological systems at a local scale: Analyzing the coupled effects of hydrochemistry and biological activity in a Fe and CO2 rich spring. *Sci. Total Environ.* **2016**, *569*, 700–715. [CrossRef]
25. Choi, H.-S.; Koh, Y.-K.; Bae, D.-S.; Park, S.-S.; Hutcheon, I.; Yun, S.-T. Estimation of deep-reservoir temperature of CO2-rich springs in Kangwon district, South Korea. *J. Volcanol. Geotherm. Res.* **2005**, *141*, 77–89. [CrossRef]

26. Choi, H.-S.; Yun, S.-T.; Koh, Y.-K.; Mayer, B.; Park, S.-S.; Hutcheon, I. Geochemical behavior of rare earth elements during the evolution of CO2-rich groundwater: A study from the Kangwon district, South Korea. *Chem. Geol.* **2009**, *262*, 318–327. [CrossRef]
27. Choi, B.-Y.; Yun, S.-T.; Kim, K.-H.; Choi, H.-S.; Chae, G.-T.; Lee, P.-K. Geochemical modeling of CO2–water–rock interactions for two different hydrochemical types of CO2-rich springs in Kangwon District, Korea. *J. Geochem. Explor.* **2014**, *144*, 49–62. [CrossRef]
28. Jeong, C.H.; Kim, H.J.; Lee, S.Y. Hydrochemistry and genesis of CO2-rich springs from Mesozoic granitoids and their adjacent rocks in South Korea. *Geochem. J.* **2005**, *39*, 517–530. [CrossRef]
29. Jeong, C.-H.; Yoo, S.-W.; Kim, K.-H.; Nagao, K. Hydrochemistry and Origin of Noble Gases and CO 2 Gas Within Carbonated Mineral Waters in the Kyeoungbuk-Kangwon Province, Korea. *J. Eng. Geol.* **2011**, *21*, 65–77. [CrossRef]
30. Choi, B.-Y. Potential impact of leaking CO2 gas and CO2-rich fluids on shallow groundwater quality in the Chungcheong region (South Korea): A hydrogeochemical approach. *Int. J. Greenh. Gas Control.* **2019**, *84*, 13–28. [CrossRef]
31. Lee, D.; Yun, S.; Kim, J. *Explanatory Text of the Geological Map of Changchon Sheet*; Sheet 6827 II, Scale 1: 50,000; Geological and Mineral Institute of Korea: Daejeon, South Korea, 1975; pp. 1–10.
32. Cheong, C.H.; Won, C.K.; Cha, M.S.; Kang, K.W.; Lee, Y.C. *Explanatory Text of the Geological Map of Odaesan Sheet (1:50,000)*; Geological and Mineral institute of Korea: Daejeon, South Korea, 1975.
33. Kim, S.; Park, B.; Kim, O.; Yoo, B.; Kim, K. *Explanatory Text of the Geological Map of Bugbunri Sheet, Sheet 6927-IV, Scale 1: 50,000*; Geological and Mineral Institute of Korea: Daejeon, South Korea, 1975; pp. 1–5.
34. Epstein, S.; Mayeda, T. Variation of O18 content of waters from natural sources. *Geochim. Cosmochim. Acta* **1953**, *4*, 213–224. [CrossRef]
35. Kendall, C.; Coplen, T.B. Multi-sample conversion of water to hydrogen by zinc for stable isotope determination. *Anal. Chem.* **1985**, *57*, 1437–1440. [CrossRef]
36. Parkhurst, B.D.L.; Appelo, C.J. User's guide to PHREEQC (version 2): A computer program for speciation, batch-reaction, one-dimensional transport, and inverse geochemical calculations. *Water-Resour. Investig. Rep.* **1999**, *99*, 312.
37. Guler, C.; Thyne, G.D.; McCray, J.E.; Turner, K.A. Evaluation of graphical and multivariate statistical methods for classification of water chemistry data. *Hydrogeol. J.* **2002**, *10*, 455–474. [CrossRef]
38. Mayo, A.L.; Loucks, M.D. Solute and isotopic geochemistry and ground water flow in the central Wasatch Range, Utah. *J. Hydrol.* **1995**, *172*, 31–59. [CrossRef]
39. Mayo, A.L.; Muller, A.B. Low temperature diagenetic–metamorphic and magmatic contributions of external CO2 gas to a shallow ground water system. *J. Hydrol.* **1997**, *194*, 286–304. [CrossRef]
40. White, W.M. *Geochemistry*; John Wiley & Sons: Hoboken, NJ, USA, 2013; ISBN 1-118-48527-0.
41. Lambrakis, N.; Kallergis, G. Contribution to the study of Greek thermal springs: Hydrogeological and hydrochemical characteristics and origin of thermal waters. *Hydrogeol. J.* **2004**, *13*, 506–521. [CrossRef]
42. Koh, Y.-K.; Choi, B.-Y.; Yun, S.-T.; Choi, H.-S.; Mayer, B.; Ryoo, S.-W. Origin and evolution of two contrasting thermal groundwaters (CO2-rich and alkaline) in the Jungwon area, South Korea: Hydrochemical and isotopic evidence. *J. Volcanol. Geotherm. Res.* **2008**, *178*, 777–786. [CrossRef]
43. Clark, I.D.; Fritz, P. Environmental Isotopes in Hydrogeology. *Environ. Isot. Hydrogeol.* **2013**. [CrossRef]
44. Deines, P.; Langmuir, D.; Harmon, R.S. Stable carbon isotope ratios and the existence of a gas phase in the evolution of carbonate ground waters. *Geochim. Cosmochim. Acta* **1974**, *38*, 1147–1164. [CrossRef]
45. Kim, K.; Jeong, G.Y. Factors influencing natural occurrence of fluoride-rich groundwaters: A case study in the southeastern part of the Korean Peninsula. *Chemosphere* **2005**, *58*, 1399–1408. [CrossRef]
46. Bernhard, G.; Geipel, G.; Reich, T.; Brendler, V.; Amayri, S.; Nitsche, H. Uranyl (VI) carbonate complex formation: Validation of the Ca2UO2(CO3)3(aq.) species. *Radiochim. Acta* **2001**, *89*, 89. [CrossRef]
47. Dong, W.; Brooks, S.C. Determination of the Formation Constants of Ternary Complexes of Uranyl and Carbonate with Alkaline Earth Metals (Mg2+, Ca2+, Sr2+, and Ba2+) Using Anion Exchange Method. *Environ. Sci. Technol.* **2006**, *40*, 4689–4695. [CrossRef]
48. Fox, P.M.; Davis, J.A.; Zachara, J.M. The effect of calcium on aqueous uranium(VI) speciation and adsorption to ferrihydrite and quartz. *Geochim. Cosmochim. Acta* **2006**, *70*, 1379–1387. [CrossRef]
49. Merkel, B.; Schipek, M. (Eds.) *The New Uranium Mining Boom: Challenge and Lessons Learned*; Springer Geology; Springer: Berlin/Heidelberg, Germany, 2012; ISBN 978-3-642-22121-7.

50. Shin, W.; Oh, J.; Choung, S.; Cho, B.-W.; Lee, K.-S.; Yun, U.; Woo, N.-C.; Kim, H.K. Distribution and potential health risk of groundwater uranium in Korea. *Chemosphere* **2016**, *163*, 108–115. [CrossRef]
51. Hwang, J. Geological review on the distribution and source of uraniferous groundwater in South Korea. *J. Eng. Geol.* **2018**, *28*, 593–603.
52. World Health Organization. *Guidelines for Drinking-Water Quality*, 4th ed.; World Health Organization: Geneva, Switzerland, 2017; ISBN 978-92-4-154995-0.
53. Cornell, R.M.; Schwertmann, U. *The Iron Oxides: Structure, Properties, Reactions, Occurrences and Uses*; John Wiley & Sons: Hoboken, NJ, USA, 2003; ISBN 3-527-30274-3.